

Electroweak Higgs effective field theory after LHC run 2

Oscar J. P. Éboli^{1,*}, M. C. Gonzalez-Garcia,^{2,3,4,†} and Matheus Martines^{1,2,‡}

¹*Instituto de Física, Universidade de São Paulo, R. do Matão 1371, 05508-090 São Paulo, Brazil*

²*Departament de Física Quantica i Astrofísica and Institut de Ciències del Cosmos,
Universitat de Barcelona, Diagonal 647, E-08028 Barcelona, Spain*

³*Institució Catalana de Recerca i Estudis Avancats (ICREA) Passeig Lluís Companys 23,
08010 Barcelona, Spain*

⁴*C.N. Yang Institute for Theoretical Physics, Stony Brook University,
Stony Brook, New York 11794-3849, USA*



(Received 6 January 2022; accepted 18 February 2022; published 14 March 2022)

We analyze the electroweak interactions in the framework of the Higgs effective field theory using the available Higgs and electroweak diboson production results from LHC run 2 as well as the electroweak precision data. Assuming universality of the weak current, our study considers 25 possible anomalous couplings. To unveil the nature of the Higgs boson, i.e., isosinglet versus part of $SU(2)_L$ doublet, we explore the correlation effects between observables that are predicted to exist in the linear realization of the electroweak gauge symmetry but not in its nonlinear counterpart. This improves previous studies aimed at investigating the Higgs nature and the origin of the electroweak symmetry breaking.

DOI: 10.1103/PhysRevD.105.053003

I. INTRODUCTION

The CERN Large Hadron Collider (LHC) has accumulated an impressive amount of data which allows not only to search for direct beyond the standard model (BSM) signals, but also to perform precision tests of the standard model (SM). Due to the lack of direct evidence of new physics, it is reasonable to assume that it is heavy. Therefore, we use effective Lagrangians [1–3] to search for deviations from the SM predictions.

The nature of the Higgs-like state observed at the LHC in 2012 [4,5] plays a pivotal role in the construction of the low-energy effective field theory. If it belongs to a $SU(2)_L$ doublet, the SM gauge symmetry can be realized linearly in the effective theory, which in this case is called standard model effective field theory (SMEFT). Conversely, if the Higgs boson is a $SU(2)_L$ isosinglet, we are led to use a nonlinear realization of the gauge symmetry and the low effective theory obtained this way is called Higgs effective field theory (HEFT); for a review of these frameworks see Ref. [6]. In a top-down approach the Wilson coefficients depend upon the specific UV-completion realized in nature.

Here, we adopt a bottom-up strategy where the Wilson coefficients are treated as free parameters, therefore, probing a large set of models simultaneously.

In this work we analyze the presently available electroweak data to study the HEFT. More specifically, we employ the Z -pole precision electroweak observables (EWPO), the diboson WW , γW , and WZ productions and the recently released Higgs kinematic distributions to constrain the HEFT Wilson coefficients. Furthermore, we also study the Higgs nature by analyzing the correlations between the diboson production and Higgs properties that are present in the linear realization of the symmetry but they are absent in the nonlinear one [7]. We also study the impact of the LHC data on a class of composite Higgs models [8–10] which introduce correlations between some of the HEFT Wilson coefficients.

Previous works analyzed the LHC HEFT phenomenology taking into account a different choice of power counting to order the HEFT series [11]; see for instance Refs. [12–19]. Generically, these works consider anomalous interactions which exhibit the same Lorentz structure of the SM. Here, we expand the list of effective operators probed in these analyses and also consider substantially updated datasets with most of the experimental results containing the full LHC run 2 luminosity. In particular we include in the analysis the most up to date results on the kinematic distributions for the Higgs observables in the form of simplified template cross sections (STXS) [20,21]. Furthermore, we not only consider constraints associated with Higgs observables but we also analyze the impact of

*eboli@if.usp.br

†maria.gonzalez-garcia@stonybrook.edu

‡matheus27martines@gmail.com

Published by the American Physical Society under the terms of the [Creative Commons Attribution 4.0 International license](#). Further distribution of this work must maintain attribution to the author(s) and the published article's title, journal citation, and DOI. Funded by SCOAP³.

the LHC run 2 data on triple electroweak gauge-boson couplings (TGCs). This allows us to quantify observables which depend on the nature of the Higgs boson. Finally, our quantification of the present status of the bounds on some specific composite Higgs models extends that of previous works [19,22–24] by considering the impact of the Higgs kinematic distributions and the full LHC run 2 dataset.

The overall picture that emerges from our analyses is that the presently available data is in agreement with the SM, as could be anticipated. This allows us to obtain stringent constraints on the Wilson coefficients parametrizing our bottom-up approach. In particular, the Higgs interactions to photon and gluon pairs receive the strongest constraints. In addition the triple electroweak gauge-boson couplings agree with the SM prediction at the percent level.

This work is organized as follows. We present in Sec. II the theoretical framework of our studies while Sec. III describes how we performed our analyses as well as the datasets used in it. Our results are presented in Sec. IV and we discuss some implication of those in Sec. V.

II. THEORETICAL FRAMEWORK

In this work we consider that the observed Higgs-like state is an isosinglet of the SM gauge symmetries. In this scenario, the realization of the SM gauge symmetries is nonlinear. Denoting the electroweak (EW) Goldstone bosons (GB) as $\vec{\pi}$, the building block of the low-energy effective Lagrangian is a dimensionless unitary matrix

$$\mathbf{U}(x) = e^{i\sigma^a \pi_a(x)/f}, \quad (2.1)$$

$$\begin{aligned} \mathcal{L}_0 = & -\frac{1}{4} \mathcal{G}_{\mu\nu}^\alpha \mathcal{G}^{\alpha\mu\nu} - \frac{1}{4} W_{\mu\nu}^a W^{a\mu\nu} - \frac{1}{4} B_{\mu\nu} B^{\mu\nu} + \frac{1}{2} \partial_\mu h \partial^\mu h - \frac{v^2}{4} \text{Tr}(\mathbf{V}_\mu \mathbf{V}^\mu) \mathcal{F}_C(h) - V(h) + i\bar{Q}_L \not{D} Q_L + i\bar{Q}_R \not{D} Q_R + i\bar{L}_L \not{D} L_L \\ & + i\bar{L}_R \not{D} L_R + -\frac{v}{\sqrt{2}} (\bar{Q}_L \mathbf{U} \mathcal{Y}_Q(h) Q_R + \text{H.c.}) - \frac{v}{\sqrt{2}} (\bar{L}_L \mathbf{U} \mathcal{Y}_L(h) L_R + \text{H.c.}), \end{aligned} \quad (2.6)$$

where L (Q) denotes the lepton (quark) fermionic field. $\mathcal{G}_{\mu\nu}^\alpha$, $W_{\mu\nu}^a$ and $B_{\mu\nu}$ stand for the $SU(3)_c$, $SU(2)_L$, and $U(1)_Y$ field strengths respectively. The covariant derivative acting on the left-handed and on the right-handed fermion fields can be generically written in the following way

$$D_\mu \psi_L = \left(\partial_\mu + ig_s T^A G_\mu^A + ig W_\mu^a \frac{\sigma^a}{2} + i \frac{g'}{2} B_\mu Y_\psi \right) \psi_L, \quad (2.7)$$

$$D_\mu \psi_R = \left(\partial_\mu + ig_s T^A G_\mu^A + i \frac{g'}{2} B_\mu (\sigma^3 + Y_\psi) \right) \psi_R. \quad (2.8)$$

The G_μ^A , W_μ^a , and B_μ represent the $SU(3)_c$, $SU(2)_L$, and $U(1)_Y$ gauge boson fields respectively. The T^A are the $SU(3)_c$ generators, the Gell-Mann matrices, with normali-

where f is the GB scale and σ^a are the Pauli matrices. \mathbf{U} transforms as a bidoublet under the global symmetry $SU(2)_L \otimes SU(2)_R$,

$$\mathbf{U} \rightarrow \mathbf{U}' = L \mathbf{U} R^\dagger, \quad (2.2)$$

with L (R) being a $SU(2)_{L(R)}$ transformation. Its covariant derivative reads

$$\mathbf{D}_\mu \mathbf{U}(x) \equiv \partial_\mu \mathbf{U}(x) + ig \frac{\sigma^j}{2} W_\mu^j(x) \mathbf{U}(x) - \frac{ig'}{2} B_\mu(x) \mathbf{U}(x) \sigma_3. \quad (2.3)$$

It is also convenient to define the vector chiral field and its covariant derivative as

$$\mathbf{V}_\mu \equiv (\mathbf{D}_\mu \mathbf{U}) \mathbf{U}^\dagger, \quad (2.4)$$

$$D_\mu \mathbf{V}_\alpha = \partial_\mu \mathbf{V}_\alpha + ig [W_\mu, \mathbf{V}_\alpha], \quad (2.5)$$

where W_μ stands for $W_\mu^j \sigma^j / 2$. We also define the scalar chiral field $\mathbf{T} \equiv \mathbf{U} \sigma_3 \mathbf{U}^\dagger$. These three objects transform in the adjoint of $SU(2)_L$.

We follow the notation defined in Ref. [25] to which we refer the reader for details in the construction of the HEFT Lagrangian. In brief, the leading order (LO) term in the HEFT expansion is

zation $\text{Tr}(T^A T^B) = 2\delta^{AB}$. In the covariant derivative of the lepton fields, the $SU(3)_c$ term must be dropped. The function $\mathcal{F}_C(h)$ can be expanded as

$$\mathcal{F}_C(h) = 1 + 2a_C \frac{h}{v} + b_C \frac{h^2}{v^2} + \dots, \quad (2.9)$$

where the dots account for higher powers of (h/v) . It is convenient to single out the BSM part of the coefficients a_C and b_C by writing

$$a_C = 1 + \Delta a_C, \quad b_C = 1 + \Delta b_C, \quad (2.10)$$

where Δa_C , and Δb_C are assumed to be of the same order as the coefficients accompanying the operators appearing in next-to-leading order (NLO) $\Delta \mathcal{L}$.

The Yukawa couplings depend on functions $\mathcal{Y}_{Q,L}(h)$ analogous to $\mathcal{F}_C(h)$, whose first two terms are

$$\begin{aligned}\mathcal{Y}_Q(h) &\equiv \text{diag}\left(Y_U^{(0)} + Y_U^{(1)} \frac{h}{v} + \dots, Y_D^{(0)} + Y_D^{(1)} \frac{h^n}{v^n} + \dots\right), \\ \mathcal{Y}_L(h) &\equiv \text{diag}\left(0, Y_\ell^{(0)} + Y_\ell^{(1)} \frac{h}{v} + \dots\right).\end{aligned}\quad (2.11)$$

The $Y^{(0)}$ terms yield fermion masses, while the $Y^{(1)}$ ones control the Higgs coupling to fermion pairs.

The BSM contributions are described by a $\Delta\mathcal{L}$ whose ordering depends upon the choice of power counting. Following Ref. [25], we consider that the NLO operators are either the ones necessary to renormalize one-loop divergences or receive finite one-loop contributions. In total, in the absence of right-handed neutrinos there are 148 independent operators that conserve CP without taking into account flavor indices.

This Lagrangian can be generically written as

$$\begin{aligned}\Delta\mathcal{L} = &\sum_i c_i \mathcal{P}_i + \sum_i n_i^Q \mathcal{N}_i^Q + \sum_i n_i^\ell \mathcal{N}_i^\ell \\ &+ \sum_i r_i^Q \mathcal{R}_i^Q + \sum_i r_i^\ell \mathcal{R}_i^\ell + \sum_i r_i^{Q\ell} \mathcal{R}_i^{Q\ell}\end{aligned}\quad (2.12)$$

for operators involving only bosons (\mathcal{P}_i), two quark or two lepton currents (\mathcal{N}^Q , and \mathcal{N}^ℓ), and four fermion currents (\mathcal{R}^Q , \mathcal{R}^ℓ and $\mathcal{R}^{Q\ell}$). Each of them includes a function $\mathcal{F}_i(h)$ conventionally parametrized as

$$\mathcal{F}_i(h) = 1 + 2\bar{a}_i \frac{h}{v} + \bar{b}_i \frac{h^2}{v^2} + \dots\quad (2.13)$$

If c_j is the Wilson coefficient of the effective operator j , it appears multiplying all the terms in the definition of \mathcal{F}_j . Therefore, for convenience, in what follows we introduce the notation

$$c_j \bar{a}_j \rightarrow a_j, \quad c_j \bar{b}_j \rightarrow b_j \dots$$

and equivalently for operators with coefficients n_j and r_j .

At this point, it is important to notice that there are not enough data to constrain all the Wilson coefficients contained in the LO and NLO Lagrangians, therefore we focus on a representative subset of operators. From the LO Lagrangian we shall consider four of the Yukawa couplings together with the bosonic operator \mathcal{F}_C . At NLO we include effects from 13 purely bosonic operators and seven operators involving fermions.

In particular we consider the ten operators that contribute to the electroweak precision data

$$\begin{aligned}\mathcal{P}_1(h) &= B_{\mu\nu} \text{Tr}(\mathbf{T}W^{\mu\nu}) \mathcal{F}_1, \quad \mathcal{P}_T(h) = \frac{v^2}{4} \text{Tr}(\mathbf{T}\mathbf{V}_\mu) \text{Tr}(\mathbf{T}\mathbf{V}^\mu) \mathcal{F}_T, \\ \mathcal{P}_{12}(h) &= (\text{Tr}(\mathbf{T}W_{\mu\nu}))^2 \mathcal{F}_{12}, \\ \mathcal{N}_1^Q &\equiv i\bar{Q}_L \gamma_\mu \mathbf{V}^\mu Q_L \mathcal{F}_{1Q}, \\ \mathcal{N}_2^Q + \mathcal{N}_8^Q &= i\bar{Q}_R \gamma_\mu \mathbf{U}^\dagger \mathbf{V}^\mu \mathbf{U} Q_R \mathcal{F}_{2Q} + i\bar{Q}_R \gamma_\mu \mathbf{U}^\dagger \mathbf{T}\mathbf{V}^\mu \mathbf{T}\mathbf{U} Q_R \mathcal{F}_{8Q}, \\ \mathcal{N}_5^Q &= i\bar{Q}_L \gamma_\mu \{\mathbf{V}^\mu, \mathbf{T}\} Q_L \mathcal{F}_{5Q}, \\ \mathcal{N}_6^Q &= i\bar{Q}_R \gamma_\mu \mathbf{U}^\dagger \{\mathbf{V}^\mu, \mathbf{T}\} \mathbf{U} Q_R \mathcal{F}_{6Q}, \\ \mathcal{N}_7^Q &= i\bar{Q}_L \gamma_\mu \mathbf{T}\mathbf{V}^\mu \mathbf{T} Q_L \mathcal{F}, \\ \mathcal{N}_2^\ell &= i\bar{L}_R \gamma_\mu \mathbf{U}^\dagger \{\mathbf{V}^\mu, \mathbf{T}\} \mathbf{U} L_R \mathcal{F}_{2\ell}, \\ \mathcal{R}_2^\ell - \mathcal{R}_5^\ell &= (\bar{L}_L \gamma_\mu L_L)(\bar{L}_L \gamma^\mu L_L) \mathcal{F}_{2L} - (\bar{L}_L \gamma_\mu \mathbf{T} L_L)(\bar{L}_L \gamma^\mu \mathbf{T} L_L) \mathcal{F}_{5L}.\end{aligned}\quad (2.14)$$

The operators \mathcal{P}_1 , \mathcal{P}_T , \mathcal{P}_{12} , and $\mathcal{R}_2^\ell - \mathcal{R}_5^\ell$ contribute to the oblique parameters S , T , U , and to a shift to the Fermi constant respectively. Moreover, the six remaining operators modify the W and Z couplings to fermion pairs. These contributions are presented in detail in Ref. [25].

Altogether in our fit to the EWPO we parametrize the HEFT contributions in terms of the following Wilson coefficients

$$\{c_1, c_T, c_{12}, n_1^Q, n_2^Q + n_8^Q, n_5^Q, n_6^Q, n_7^Q, n_2^\ell, r_2^\ell - r_5^\ell\}, \quad (2.15)$$

which correspond to the contributing part of the operators in Eq. (2.14) by taking $\mathcal{F} = 1$.

In addition, we consider four bosonic operators that modify the TGC and affect the production of electroweak gauge boson pairs W^+W^- , $W^\pm Z$, and $W^\pm\gamma$ at the LHC,

$$\begin{aligned}
\mathcal{P}_2(h) &= \frac{i}{4\pi} B_{\mu\nu} \text{Tr}(\mathbf{T}[\mathbf{V}^\mu, \mathbf{V}^\nu]) \mathcal{F}_2, \\
\mathcal{P}_3(h) &= \frac{i}{4\pi} \text{Tr}(W_{\mu\nu}[\mathbf{V}^\mu, \mathbf{V}^\nu]) \mathcal{F}_3, \\
\mathcal{P}_{13}(h) &= \frac{i}{4\pi} \text{Tr}(\mathbf{T}W_{\mu\nu}) \text{Tr}(\mathbf{T}[\mathbf{V}^\mu, \mathbf{V}^\nu]) \mathcal{F}_{13}, \\
\mathcal{P}_{WWW}(h) &= \frac{4\pi e_{abc}}{\Lambda^2} W_\mu^{a\nu} W_\nu^{b\rho} W_\rho^{c\mu} \mathcal{F}_{WWW}, \tag{2.16}
\end{aligned}$$

whose correspondent Wilson coefficients for $\mathcal{F} = 1$ are

$$\{c_2, c_3, c_{13}, c_{WWW}\}. \tag{2.17}$$

These operators modify the TGC $\gamma W^+ W^-$, and $Z W^+ W^-$. These anomalous contributions can be generically parametrized in terms of the usual effective TGC Lagrangian given in Ref. [26],

$$\begin{aligned}
\mathcal{L}_{WWW} = -ig_{WWW} \Bigg\{ & g_1^V (W_{\mu\nu}^+ W^{-\mu} V^\nu - W_\mu^+ V_\nu W^{-\mu\nu}) \\
& + \kappa_V W_\mu^+ W_\nu^- V^{\mu\nu} + \frac{\lambda_V}{2m_W^2} W_{\mu\nu}^+ W^{-\nu\rho} V_\rho^\mu \Bigg\}, \tag{2.18}
\end{aligned}$$

with deviations from the SM predictions $g_1^Z = \kappa_Z = \kappa_\gamma = 1$, $\lambda_\gamma = \lambda_Z = 0$,

$$\begin{aligned}
\Delta g_1^Z &= g_1^Z - 1 \equiv \frac{g}{4\pi c_W^2} c_3, \\
\Delta \kappa_Z &= \kappa_Z - 1 \equiv \frac{g}{4\pi} (c_3 + 2c_{13} - 2t_W c_2), \\
\Delta \kappa_\gamma &= \kappa_\gamma - 1 \equiv \frac{g}{4\pi} \left(c_3 + 2c_{13} + 2\frac{c_2}{t_W} \right), \\
\lambda_\gamma &= \lambda_Z \equiv \frac{6\pi g v^2}{\Lambda^2} c_{WWW}, \tag{2.19}
\end{aligned}$$

where c_W (t_W) stands for $\cos \theta_W$ ($\tan \theta_W$). Electromagnetic gauge invariance enforces $g_1' = 1$, both in the SM and in the presence of the new operators. In Eq. (2.18), $V \equiv \{\gamma, Z\}$, $g_{WW\gamma} = e$, $g_{WWZ} = g \cos \theta_W$, and $W_{\mu\nu}^\pm$ and $V_{\mu\nu}$ refer exclusively to the kinetic part of the gauge field strengths.

Concerning Higgs processes, eleven additional operators take part in our Higgs couplings analysis. They originate from the part proportional to Δa_C of the operator \mathcal{F}_C and the deviations of the Yukawa couplings $[Y_f^{(1)}]$ for the top, bottom, tau, and muon in Eq. (2.6) as well as the NLO bosonic operators

$$\begin{aligned}
\mathcal{P}_4(h) &= \frac{i}{4\pi} B_{\mu\nu} \text{Tr}(\mathbf{T}V^\mu) \partial^\nu \mathcal{F}_4, \\
\mathcal{P}_5(h) &= \frac{i}{4\pi} \text{Tr}(W_{\mu\nu} V^\mu) \partial^\nu \mathcal{F}_5, \\
\mathcal{P}_{17}(h) &= \frac{i}{4\pi} \text{Tr}(\mathbf{T}W_{\mu\nu}) \text{Tr}(\mathbf{T}V^\mu) \partial^\nu \mathcal{F}_{17}, \\
\mathcal{P}_B(h) &= -\frac{1}{4} B_{\mu\nu} B^{\mu\nu} \mathcal{F}_B, \\
\mathcal{P}_W(h) &= -\frac{1}{4} W_{\mu\nu}^a W^{a\mu\nu} \mathcal{F}_W, \\
\mathcal{P}_G(h) &= -\frac{1}{4} G_{\mu\nu}^a G^{a\mu\nu} \mathcal{F}_G. \tag{2.20}
\end{aligned}$$

The corresponding Wilson coefficients characterizing the strength of the effective interaction that enter in the Higgs analysis are

$$\{a_4, a_5, a_{17}, a_B, a_W, a_G\}. \tag{2.21}$$

We notice that, in principle, $a_{T(1)}$ also affects the Higgs couplings. However, we anticipate here that the EWPO will set strong bounds on $c_{T(1)}$, and consequently, under the assumption that the corresponding $\bar{a}_{T(1)}$ couplings are at most $\mathcal{O}(1)$, we can safely neglect their contribution. Notice also that, for the sake of simplicity, we have not considered the deviation on Higgs quartic vertices ($H V f \bar{f}'$) generated by some of the fermion current operators.

As we will see in the following section, at present there is enough experimental information to individually bound the 20 Wilson coefficients in Eqs. (2.15), (2.17), and (2.21) as well as four Yukawa couplings and Δa_C . However, the analysis, in particular when performed up to quadratic order in the coefficients, can potentially exhibit discrete (quasi-) degeneracies associated to sign flips of the SM Higgs couplings. For example, the vertex $H V^\mu V_\mu$ ($V = W^\pm$ or Z) is proportional to [25]

$$1 + \Delta a_C \tag{2.22}$$

therefore, we can anticipate a degeneracy with the SM results for the $H V^\mu V_\mu$ vertex ($\Delta a_C = 0$) for $\Delta a_C = -2$.

In similar fashion, the anomalous interactions can also lead to Yukawa couplings of the order of the SM ones but with a different sign because the coefficient of the $H \bar{f} f$ vertex is now

$$\frac{1}{\sqrt{2}} Y_f^{(1)} = \frac{1}{\sqrt{2}} Y_f^{(0)} \left(\frac{Y_f^{(1)}}{Y_f^{(0)}} \right), \tag{2.23}$$

and, therefore, it presents one degenerate solution $\frac{Y_f^{(1)}}{Y_f^{(0)}} = -1$ with the SM one $\frac{Y_f^{(1)}}{Y_f^{(0)}} = +1$.

Another source of degeneracy is the effective photon-photon-Higgs coupling that gets corrections from by \mathcal{P}_W and \mathcal{P}_B ,

$$-\frac{1}{4}G_{\text{SM}}^{\gamma\gamma} + \frac{1}{2v}(a_B c_W^2 + a_W s_W^2), \quad (2.24)$$

where $G_{\text{SM}}^{\gamma\gamma} \simeq 3.3 \times 10^{-2}$ is the one-loop SM contribution. Consequently, a SM-like solution for the Higgs decay into $\gamma\gamma$ can be found for $a_B c_W^2 + a_W s_W^2 \simeq v G_{\text{SM}}^{\gamma\gamma} \simeq 8.4 \times 10^{-3}$.

A similar effect is also present in $H\mathcal{G}^{\mu\nu}\mathcal{G}_{\mu\nu}$ whose coupling in the large top mass limit is

$$-\frac{1}{4}G_{\text{SM}}^{gg}\left(\frac{Y_t^{(1)}}{Y_t^{(0)}}\right) - \frac{1}{2v}a_G, \quad (2.25)$$

with $G_{\text{SM}}^{gg} \simeq 5.3 \times 10^{-2} \text{ TeV}^{-1}$ being the one-loop SM contribution.

It is important to notice that the effective operators entering the degeneracies in Eqs. (2.22)–(2.25) lead to distinct Higgs kinematic distributions either due to a different number of derivatives of the Higgs field or their contribution to the one-loop Higgs coupling to gluon pairs [27]. Therefore, we anticipate that some of the potential degeneracies can be resolved by the available data on the Higgs kinematic distributions, as we will see in Sec. IV.

As it is well known, when the electroweak gauge symmetry is linearly realized in the low-energy effective theory, the Higgs boson is part of a $SU(2)_L$ doublet as in the SM. This is the scenario described by the SMEFT. The comparison between the results of the analyses performed in the frameworks of HEFT and SMEFT allows us to probe the nature of the Higgs boson [7]. A particularly sensitive probe is associated with the (de)correlation of the contributions to the TGC and Higgs-gauge-boson couplings in the two scenarios. In brief, in SMEFT the following operators induce anomalous triple-gauge boson couplings

$$\begin{aligned} \mathcal{O}_W &= \frac{ig}{2}(D_\mu\Phi)^\dagger W^{\mu\nu}(D_\nu\Phi), \\ \mathcal{O}_B &= \frac{ig'}{2}(D_\mu\Phi)^\dagger B^{\mu\nu}(D_\nu\Phi), \end{aligned} \quad (2.26)$$

and, in this framework, the linear realization of the gauge symmetry implies that the same operators give rise to correlated corrections to the Higgs couplings to the electroweak vector bosons. On the contrary, in HEFT there are four sibling operators, two of them, \mathcal{P}_2 and \mathcal{P}_3 , giving the corresponding corrections to the TGC (proportional to

c_2 and c_3) and the other two, \mathcal{P}_4 and \mathcal{P}_5 , inducing the corresponding shift for the HVV vertex (proportional to a_4 and a_5). It is clear then that in HEFT there is no *a priori* connection between the corrections to the TGC and the HVV vertices.

Following Refs. [7,25] we construct four specific combinations of the coefficients c_2 , c_3 , a_4 , and a_5 which are useful for quantifying the status of these (de)correlations in the Higgs and TGC results

$$\begin{aligned} \Sigma_B &\equiv \frac{1}{\pi g t_W}(2c_2 + a_4), & \Sigma_W &\equiv \frac{1}{2\pi g}(2c_3 - a_5), \\ \Delta_B &\equiv \frac{1}{\pi g t_W}(2c_2 - a_4), & \Delta_W &\equiv \frac{1}{2\pi g}(2c_3 + a_5). \end{aligned} \quad (2.27)$$

These four parameters were defined in such a way that, at dimension-six order in the SMEFT expansion, the two Δ 's are zero because of gauge invariance and of the doublet nature of the Higgs, $\Delta_B = \Delta_W = 0$. Moreover, the Σ 's are directly related to the Wilson coefficients of the operators \mathcal{O}_W and \mathcal{O}_B ; $\Sigma_B = v^2 \frac{f_B}{\Lambda^2}$ and $\Sigma_W = v^2 \frac{f_W}{\Lambda^2}$, being f_i the associated Wilson coefficient. In contrast, the HEFT operators can generate independent modifications to each of these four variables. Therefore, the study of these parameters can shed light on the nature of the Higgs boson.

In a top-down approach, we also analyze the minimal composite Higgs scenario [10,28] that is based on global symmetry $SO(5)$ broken to $SO(4)$ at scale f . In this model the Higgs interaction to vector bosons is modified with respect to the SM by a multiplicative factor

$$a_C = \sqrt{1 - \xi} \quad (2.28)$$

with $\xi = v^2/f^2$. The modification to the Higgs couplings to fermions

$$c_p \equiv \frac{Y_p^{(1)}}{Y_p^{(0)}}, \quad (2.29)$$

depends on how the SM fermions are embedded in the UV-theory. Here, following [23], we consider the two characteristic choices labeled A and B ,

$$c_p^A = \sqrt{1 - \xi} \quad \text{or} \quad c_p^B = \frac{1 - 2\xi}{\sqrt{1 - \xi}}, \quad (2.30)$$

where in the equations above p stands for top, bottom, tau and muon in our analysis.

III. ANALYSIS FRAMEWORK

In order to obtain the present constraints on HEFT, we considered the available data on the EWPO, the triple electroweak gauge couplings and the Higgs data. In the

EWPO data analysis, we analyze 15 observables of which 12 are Z observables [29],

$$\begin{aligned} \Gamma_Z, \quad \sigma_h^0, \quad \mathcal{A}_\ell(\tau^{\text{pol}}), \quad R_\ell^0, \quad \mathcal{A}_\ell(\text{SLD}), \quad A_{\text{FB}}^{0,l}, \\ R_c^0, \quad R_b^0, \quad \mathcal{A}_c, \quad \mathcal{A}_b, \quad A_{\text{FB}}^{0,c}, \quad \text{and} \quad A_{\text{FB}}^{0,b}(\text{SLD/LEP-I}), \end{aligned} \quad (3.1)$$

supplemented by three W observables; the W mass (M_W) taken from [30], its width (Γ_W) from LEP2/Tevatron [31] and the leptonic W branching ratio [$\text{Br}(W \rightarrow \ell\nu)$] [30]. In our statistical analysis we define the chi-square function

$$\chi^2_{\text{EWPO}}(c_1, c_T, c_{12}, n_1^Q, n_2^Q + n_8^Q, n_5^Q, n_6^Q, n_7^Q, n_2^\ell, r_2^\ell - r_5^\ell) \quad (3.2)$$

and fitted the relevant Wilson coefficients. Notice that we assumed the couplings to be generation independent and diagonal in flavor space; for further details on this analysis see Ref. [25].

In order to study the triple couplings of electroweak gauge bosons we considered electroweak-diboson data (EWDBD) from LHC, more specifically the diboson production of WZ , WW , and $W\gamma$ pairs as well as the vector boson fusion production of Zs (Zjj). The specific data employed in our study is presented in the top rows of Table I. In total we considered 73 data points in this analysis.

The theoretical predictions were obtained by simulating the W^+W^- , $W^\pm Z$, $W^\pm\gamma$, and Zjj channels that receive

contributions from TGC. To this end, we used `MadGraph5_aMC@NLO` [48] with the Universal FeynRules Output (UFO) files for our effective Lagrangian generated with `FEYNRULES` [49,50]. We employ `PYTHIA8` [51] to perform the parton shower and hadronization, while the fast detector simulation is carried out with `DELPHES` [52]. Jet analyses were performed using `FASTJET` [53].

These predictions are statistically confronted with the LHC run 2 data by constructing a binned log-likelihood function based on the data contents of the different bins in the kinematic distribution of each channel. We consistently take into account not only the statistical errors but also the systematic and theoretical uncertainties adding them in quadrature and assuming some partial correlation among them which we estimate with the information provided by the experiments.

For the sake of simplicity in our EWDBD analysis we discarded possible effects from anomalous couplings of gauge bosons to fermion pairs, which are well constrained by the EWPO data so we have

$$\chi^2_{\text{TGC}}(c_2, c_3, c_{13}, c_{WWW}). \quad (3.3)$$

We also study the implications for HEFT of the available Higgs data. We consider the Higgs kinematic distributions for the channels that are available in the simplified template cross section (STXS) format, otherwise we use the total signal strength (SS) results. We summarize in the lower part of Table I the Higgs data we take into account, specifying its STXS or SS format. Let us notice that the correlations among the CMS STXS data for the different final states is

TABLE I. Diboson and Higgs data from LHC used in the analyses. For the W^+W^- results from ATLAS run 2 [32] we combined the data from the last three bins into one to ensure Gaussianity.

	Channel (a)	Distribution	# bins	Data set	Int Lum
EWDBD	$WZ \rightarrow \ell^+\ell^-\ell'^\pm$	$M(WZ)$	7	CMS 13 TeV,	137.2 fb^{-1} [33]
	$WW \rightarrow \ell^+\ell^{(\prime)-} + 0/1j$	$M(\ell^+\ell^{(\prime)-})$	11	CMS 13 TeV,	35.9 fb^{-1} [34]
	$W\gamma \rightarrow \ell\nu\gamma$	$\frac{d^2\sigma}{dp_T d\phi}$	12	CMS 13 TeV,	137.1 fb^{-1} [35]
	$WW \rightarrow e^\pm\mu^\mp + \cancel{E}_T(0j)$	m_T	17 (15)	ATLAS 13 TeV,	36.1 fb^{-1} [32]
	$WZ \rightarrow \ell^+\ell^-\ell'^\pm$	m_T^{WZ}	6	ATLAS 13 TeV,	36.1 fb^{-1} [36]
	$Zjj \rightarrow \ell^+\ell^-jj$	$\frac{d\sigma}{d\phi}$	12	ATLAS 13 TeV,	139 fb^{-1} [37]
	$WW \rightarrow \ell^+\ell^{(\prime)-} + \cancel{E}_T(1j)$	$\frac{d\sigma}{dm_{\ell^+\ell^-}}$	10	ATLAS 13 TeV,	139 fb^{-1} [38]
HIGGS	$H \rightarrow \tau^+\tau^-, W^+W^-, b\bar{b}(\text{VBF}, ttH + tH)$	SS	7	ATLAS at 13 TeV [Figs. 5,6]	36.1–139 [39]
	$H \rightarrow \gamma Z$	SS	1	ATLAS at 13 TeV	139 [40]
	$H \rightarrow \mu^+\mu^-$	SS	1	ATLAS at 13 TeV	139 [41]
	$H \rightarrow \gamma\gamma, ZZ, b\bar{b}(\text{VH})$	STXS	43	ATLAS at 13 TeV	139 [42]
	$H \rightarrow ZZ, b\bar{b}, \tau^+\tau^-(\text{VH}, ttH), W^+W^-(\text{ggH}, \text{VBF}, ttH)$	SS	16	CMS at 13 TeV [Table 5]	35.9–137 [43]
	$H \rightarrow \gamma Z$	SS	1	CMS at 13 TeV	139 [44]
	$H \rightarrow \gamma\gamma$	STXS	17	CMS at 13 TeV	137 [45]
	$H \rightarrow \tau^+\tau^-(\text{ggH}, \text{VBF})$	STXS	11	CMS at 13 TeV	137 [46]
	$H \rightarrow W^+W^-(\text{VH})$	STXS	4	CMS at 13 TeV	137 [47]

not publicly available. These are expected to be important for the channels $\gamma\gamma$ and $\ell\ell\ell\ell$. So, to make the analysis more robust we have conservatively chosen not to include the CMS STXS data for $\ell\ell\ell\ell$ for which we only consider the total SS for this final state.

We evaluate the theoretical predictions for the Higgs production by gluon fusion in the channels tagged as STXS in Table I using MadGraph5_aMC@NLO [54] with the SMEFT@NLO UFO files [55]. Furthermore, the STXS 1.2 classification was performed using RIVET [56].

The statistical comparison of the HEFT predictions for the Higgs run 2 data is carried out using the χ^2_{Higgs} function

$$\chi^2_{\text{Higgs}}(\Delta a_C, a_4, a_5, a_{17}, a_B, a_W, a_G, Y_t^{(1)}, Y_b^{(1)}, Y_\tau^{(1)}, Y_\mu^{(1)}), \quad (3.4)$$

which depends on 11 Wilson coefficients. Once again, we do not take into account the contributions from the anomalous gauge boson couplings to fermion pairs due to the stringent bounds emanating from the EWPO data on these couplings.

IV. RESULTS

As discussed above, in HEFT the nonlinear realization of the gauge symmetry allows for independent statistical analyses of the datasets involving corrections to the gauge-boson-fermion and gauge-boson self couplings (EWPO and TGC) and the Higgs interactions since the couplings impacting these two sectors are not connected.

	c_1	c_T	c_{12}	n_1^Q	$n_2^Q + n_8^Q$	n_5^Q	n_6^Q	n_7^Q	n_2^ℓ	$(r_2^\ell - r_5^\ell) \frac{v^2}{\Lambda^2}$
b.f. ($\times 10^{-3}$)	1.1	-1.2	-0.21	-1.5	-12	-0.20	4.4	-0.78	0.45	-0.0027
σ ($\times 10^{-3}$)	0.85	11.	5.4	1.7	5.2	0.67	2.2	1.7	0.33	0.069
95% C.L. ($\times 10^{-3}$)	(-0.66, 2.7)	(-23, 21)	(-11, 11)	(-4.9, 2.0)	(-22, -1.5)	(-1.2, 1.2)	(-0.024, 8.8)	(-4.2, 2.7)	(-0.2, 1.1)	(-0.14, 0.13)
ρ	c_1	1.000	-0.136	-0.074	0.108	-0.128	-0.075	0.019	0.113	0.950
	c_T	-0.136	1.000	0.998	0.325	0.009	0.012	0.004	-0.362	-0.130
	c_{12}	-0.074	0.998	1.000	0.333	-0.002	0.009	0.008	-0.359	-0.071
	n_1^Q	0.108	0.325	0.333	1.000	0.385	0.146	-0.077	-0.602	0.138
	$n_2^Q + n_8^Q$	-0.128	0.009	-0.002	0.385	1.000	0.042	-0.467	0.384	-0.047
	n_5^Q	-0.075	0.012	0.009	0.146	0.042	1.000	0.640	0.146	-0.098
	n_6^Q	0.019	0.004	0.008	-0.077	-0.467	0.640	1.000	-0.077	-0.045
	n_7^Q	0.113	-0.362	-0.359	-0.602	0.384	0.146	-0.077	1.000	0.142
	n_2^ℓ	0.950	-0.130	-0.071	0.138	-0.047	-0.098	-0.045	0.142	1.000
	$(r_2^\ell - r_5^\ell) \frac{v^2}{\Lambda^2}$	0.006	-0.991	-0.997	-0.346	-0.001	-0.001	0.000	0.347	0.006

Altogether, the overall picture is that there is a good agreement with the standard model. As discussed in Ref. [25], there are two main differences with respect to the corresponding analysis to EWPO obtained assuming SMEFT with operators up to dimension six, which are straight forward to identify by working in the Hagiwara, Ishihara, Szalapski, and Zeppenfeld (HISZ) basis [57,58]

A. Constraints from EWPO

We start our analysis focusing on the HEFT operators in Eq. (2.14) that contribute to the EWPO. The results are graphically presented in Fig. 1 which depicts the one- and two-dimensional projections of $\Delta\chi^2_{\text{EWPO}}$ as a function of the Wilson coefficients after marginalizing over those not displayed in each panel.

More quantitatively, the corresponding best values, uncertainties, 95% C.L. ranges, and correlations are presented in Eq. (4.2). As the EWPO analysis was performed including only the linear contribution on the Wilson coefficients (here denoted generically f_i) to the observables, by definition $\Delta\chi^2$ takes the form

$$\Delta\chi^2 = \sum_{i=1}^N (f_i - f_i^0) V_{ij}^{-1} (f_j - f_j^0), \quad (4.1)$$

where f_j^0 defines the best fit point and V is the covariance matrix

$$V_{ij} \equiv \sigma_i \sigma_j \rho_{ij},$$

with σ_j being the uncertainties and ρ_{ij} the correlation matrix. For the EWPO analysis we find the best-fit values, uncertainties and correlation matrix,

$$. \quad (4.2)$$

(see for example Refs. [59–62]): (i) in the SMEFT no contribution to the U parameter is generated at dimension six while in the HEFT c_{12} gives contribution to U , (ii) assuming universality in the gauge-fermion couplings, the W and Z couplings to fermions are linked in the SMEFT and receive contributions from the coefficients of five nonoblique operators while in the HEFT an

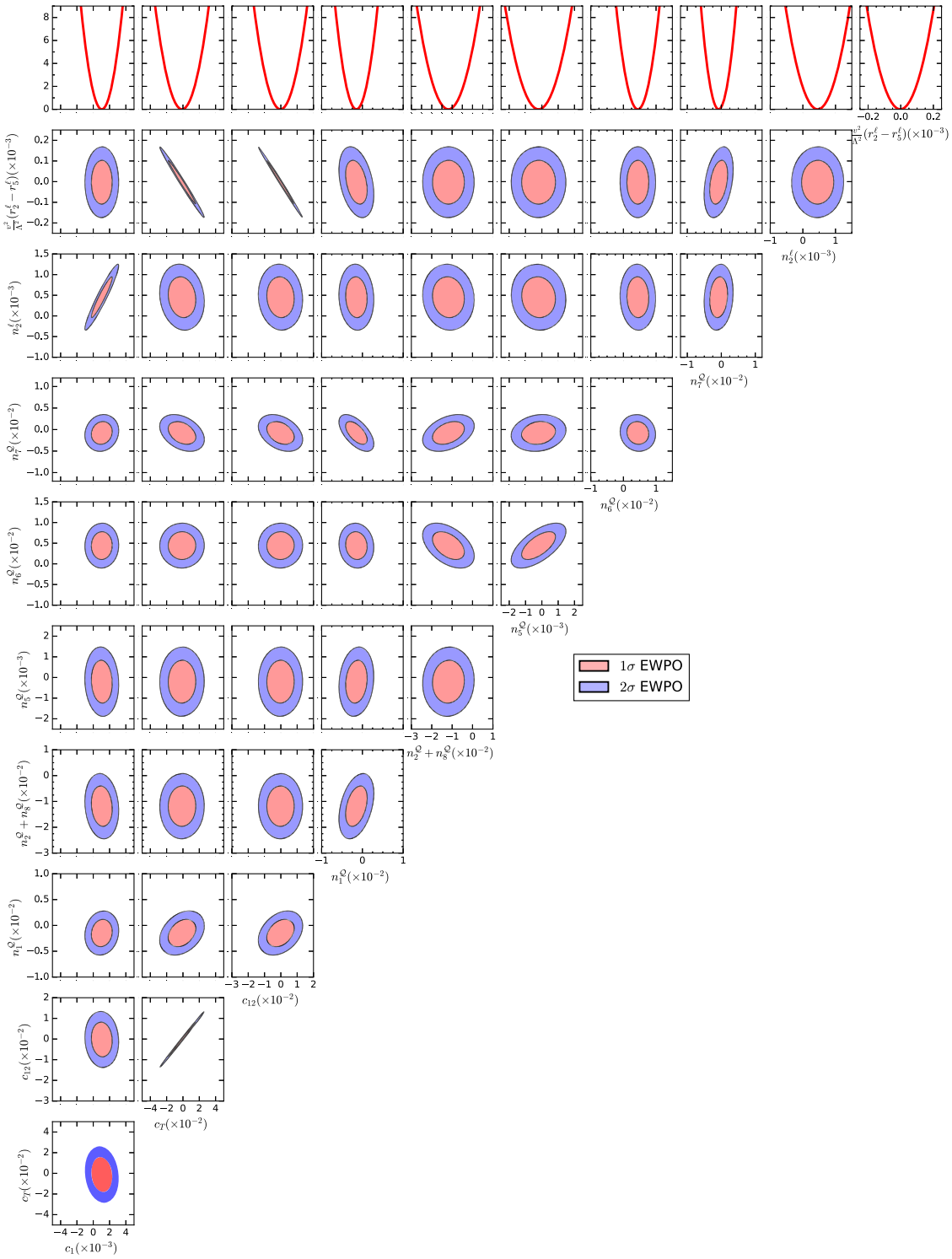


FIG. 1. One- and two-dimensional marginalized projections of $\Delta\chi^2_{\text{EWPO}}$ for the Wilson coefficients c_1 , c_T , c_{12} , n_1^Q , $n_2^Q + n_4^Q$, n_5^Q , n_6^Q , n_7^Q , n_2^{ℓ} , and $r_2^{\ell} - r_5^{\ell}$, as indicated in the panels after marginalizing over the remaining fit parameters.

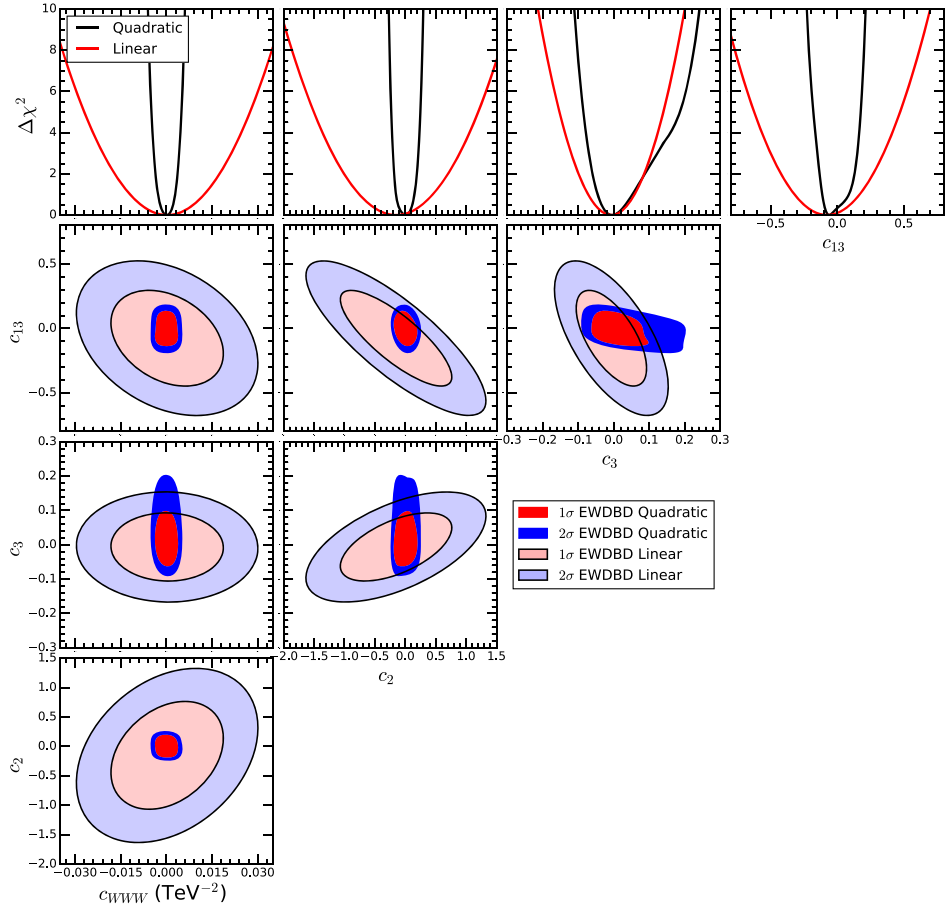


FIG. 2. One- and two-dimensional marginalized projections of $\Delta\chi^2_{\text{TGC}}$ for the Wilson coefficients c_2 , c_3 , c_{WWW} , and c_{13} as indicated in the panels after marginalizing over the remaining fit parameters. The results are shown for analyses including only the linear contributions of the Wilson coefficients (red curves and lighter regions) as well as up to quadratic contributions (black lines and darker regions).

additional nonoblique operator coefficient (n_7^Q) allows for independent variations of the W and Z couplings to quarks.

As seen in Fig. 1 and Eq. (4.2), a nonzero c_{12} has most effect on the allowed ranges of c_T and $(r_2^\ell - r_5^\ell) \frac{v^2}{\Lambda^2}$, which are the Wilson coefficients with which c_{12} is mostly correlated. This is due to possible cancellations between the oblique contributions and δG_F in the Z observables and ΔM_W ; see Ref. [25] for further details. Notice that these cancellations are possible at NLO in the HEFT but not in the SMEFT at dimension six [25]. This results into a weakening of the bounds on c_T and $(r_2^\ell - r_5^\ell) \frac{v^2}{\Lambda^2}$ by about a factor ~ 20 , though they still remain constrained at the percent and per mil level respectively.

Conversely, the contribution of the quark-current operator \mathcal{N}_7^Q has a more modest quantitative impact. In fact, it is still the case that the EWPO analysis favors nonvanishing values for the coefficients contributing to the

down-quark couplings to the Z , in particular $(\mathcal{N}_2^Q + \mathcal{N}_8^Q)$, at 2σ . This is a well-known result driven by the 2.7σ discrepancy between the observed $A_{FB}^{0,b}$ and the SM.

B. Triple gauge couplings constraints

The results of our analyses of the EWDBD are graphically presented in Fig. 2. As mentioned in Sec. III, for the sake of simplicity in our EWDBD analysis, we discard possible effects from anomalous couplings of gauge bosons to fermion pairs, which are well constrained by the EWPO data, and focus on the constraints on the bosonic operators \mathcal{P}_2 , \mathcal{P}_3 , \mathcal{P}_{13} , and \mathcal{P}_{WWW} .

We perform the EWDBD analyses considering only the linear contributions of the Wilson coefficients to the observables as well as including up to quadratic contributions. At linear order $\Delta\chi^2_{\text{TGC}}$ takes the form of Eq. (4.1) with best fit, uncertainties and correlations

		c_2	c_3	c_{13}	$c_{WWW}/(\text{TeV}^{-2})$	
	b.f.	-0.15	-0.0063	-0.076	0.00024	
	σ	0.60	0.065	0.24	0.012	
ρ	c_2	1.000	0.515	-0.855	0.275	.
	c_3	0.515	1.000	-0.675	-0.075	
	c_{13}	-0.855	-0.675	1.000	-0.365	
	$\frac{c_{WWW}}{(\text{TeV}^{-2})}$	0.275	-0.075	-0.365	1.000	

The corresponding 95% C.L. allowed ranges for both analysis are listed in Table II.

From Fig. 2 or Eq. (4.3) we can see that c_2 , c_3 , and c_{13} are strongly correlated in the linear analysis due to their contributions to the ZWW and γWW vertices through $\Delta\kappa_Z$ and $\Delta\kappa_\gamma$; see Eq. (2.19). It is interesting to notice that the $W\gamma$ production plays a significant role in constraining c_{WWW} at linear order due to the use of kinematic distributions designed to avoid the cancellation of its linear contribution [63,64].

When compared to the corresponding EWDBD analysis performed in the framework of SMEFT at dimension six in the HISZ basis [57,58], the main difference is the contribution of the operator \mathcal{P}_{13} which has no linear sibling at dimension six. As seen in Fig. 1, the presence of this additional coefficient leads to the relaxation of the bounds on c_2 (and less significantly on c_3) obtained when considering only linear contributions, as a consequence of the mentioned correlations. We also see that once the effects of the operators are included to quadratic order in the

coefficients, the inclusion of c_{13} in the analysis has minimal impact on the determination of the other three coefficients. Furthermore, the quadratic analysis leads to stronger limits by a factor of 3–5; see Table II.

C. Higgs couplings

The results of our analysis of the Higgs results are graphically presented in Figs. 3–5. As mentioned in Sec. III, we assume that $\bar{a}_{T(1)}$ couplings are at most $\mathcal{O}(1)$ and neglect the contributions from $a_{T(1)} = c_{T(1)}\bar{a}_{T(1)}$ to the Higgs observables after imposing the strong constraints on $c_{T(1)}$ from EWPO. Thus, we perform an analysis in terms of the 11 coefficients in Eq. (3.4).

We have carried out the Higgs analyses considering only the linear contributions of the Wilson coefficients to the observables as well as including up to quadratic contributions. The one-dimensional projections are depicted in Fig. 3. First of all, notice that the results are compatible with the SM at 95% C.L. in both the linear and the

TABLE II. Marginalized 95% C.L. allowed ranges for the Wilson coefficients of the operators constrained by the analysis of LHC EWDBD and Higgs results.

	95% C.L. Range	
	Linear	Quadratic
c_2	(-1.4, 1.0)	(-0.21, 0.23)
c_3	(-0.14, 0.12)	(-0.080, 0.16)
c_{13}	(-0.57, 0.41)	(-0.16, 0.16)
c_{WWW}/TeV^{-2}	$(-2.4, 2.5) \times 10^{-2}$	$(-4.6, 4.6) \times 10^{-3}$
a_4	(-0.17, 1.10)	(-0.12, 0.44)
a_5	(-0.38, 0.83)	(-0.70, 0.71)
a_{17}	(-0.38, 0.35)	(-0.49, 0.30)
a_B	$(-0.71, 3.2) \times 10^{-2}$	$(-0.53, 2.4) \times 10^{-2}$
a_W	$(-10, 2.3) \times 10^{-2}$	$(-5.5, 1.8) \times 10^{-2}$
a_G	$(-1.1, 0.37) \times 10^{-3}$	$(-1.2, 0.38) \times 10^{-3}$
Δa_C	(-0.20, 0.046)	(-0.17, 0.062)
$Y_t^{(1)}/Y_t^{(0)} - 1$	(-0.17, 0.29)	(-0.14, 0.28)
$Y_b^{(1)}/Y_b^{(0)} - 1$	(-0.50, 0.15)	$(-2.1, -1.6) \cup (-0.42, 0.13)$
$Y_\tau^{(1)}/Y_\tau^{(0)} - 1$	(-0.37, 0.062)	$(-2.0, -1.6) \cup (-0.35, 0.026)$
$Y_\mu^{(1)}/Y_\mu^{(0)} - 1$	(-0.60, 0.54)	$(-2.4, -1.1) \cup (-0.87, 0.39)$

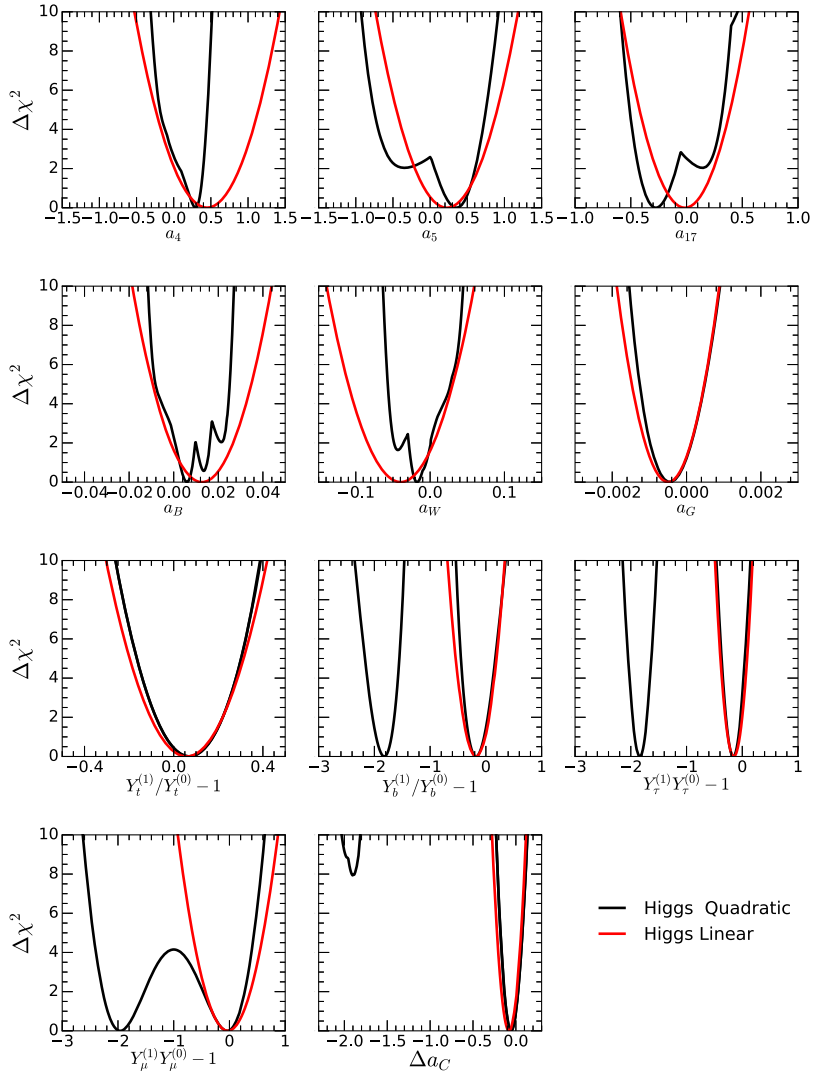


FIG. 3. $\Delta\chi^2$ as a function of the Wilson coefficients $a_4, a_5, a_{17}, a_B, a_W, a_G, Y_t^{(1)}, Y_b^{(1)}, Y_\tau^{(1)}, Y_\mu^{(1)}$, and Δa_C as indicated in the panels after marginalizing over the remaining fit parameters. The red (black) line stands for the analysis considering the linear (and quadratic) contributions of the Wilson coefficients.

quadratic analyses. Moreover, the figure shows that the dominant source of degeneracy that remains in these parameters using the LHC run 2 data are those related to the Yukawa couplings $Y_f^{(1)}$ for $f = b, \tau$ and μ , which are associated to the reversing of the SM Yukawa coupling sign; see Eq. (2.23). As seen in this figure, for the quadratic analysis Δa_C presents a second minima around $\Delta a_C \sim 2$ which is associated with the change of sign of the $H V^\mu V_\mu$ in Eq. (2.22) but it lays at $\Delta\chi^2 \sim 8$. This degeneracy is mainly broken by the tH data which receives contribution from both $H V V$ and $H t \bar{t}$ vertices while only the first one changes sign for $\Delta a_C \sim 2$. Correspondingly the degeneracy for $Y_t^{(1)} = -Y_t^{(0)}$ is also broken and in this case the solution with inverted SM sign lays at $\Delta\chi^2 \gg 10$. This is so because the top Yukawa coupling also contributes to the gluon-gluon-Higgs production in Eq. (2.25) and it can be resolved

by the STXS data. Similarly, no degenerate solution is found for a_G . In summary, the larger available luminosity as well as Higgs kinematic distributions eliminates the degeneracies associated to a_G and $Y_t^{(1)}$ that were observed previously [7].

Finally, there remain the quasidegenerate solutions associated to the \mathcal{P}_W and \mathcal{P}_B corrections to the $H\gamma\gamma$ vertex in Eq. (2.24) for which the data only constrain its modulus. This is displayed in Fig. 4 where we show the marginalized two-dimensional projections of $\Delta\chi^2_{\text{Higgs}}$ for the coefficients a_W and a_B . For the sake of clarity, we plot the allowed regions for the combinations $c_W^2 a_B + s_W^2 a_W$ (which corrects $HF^{\mu\nu}F_{\mu\nu}$) and $s_W^2 a_B - c_W^2 a_W$ (which gives a contribution to $HZ^{\mu\nu}Z_{\mu\nu}$). In the figure we clearly see the two SM-line solutions around $c_W^2 a_B + s_W^2 a_W \sim 0$, and $c_W^2 a_B + s_W^2 a_W \sim vG_{\text{SM}}^{\gamma\gamma} \simeq 0.0084$.

One thing to notice is that, when the analysis is preformed at linear order, $\Delta\chi^2_{\text{Higgs}}$ takes the form of Eq. (4.1) with best fit, uncertainties and correlations

	a_4	a_5	a_{17}	a_B	a_W	a_G	Δa_C	$\frac{Y_t^{(1)}}{Y_t^{(0)}} - 1$	$\frac{Y_b^{(1)}}{Y_b^{(0)}} - 1$	$\frac{Y_\tau^{(1)}}{Y_\tau^{(0)}} - 1$	$\frac{Y_\mu^{(1)}}{Y_\mu^{(0)}} - 1$
b.f.	0.45	0.22	-0.015	0.013	-0.040	-0.00050	-0.080	0.058	-0.17	-0.15	-0.028
σ	0.31	0.30	0.18	0.0099	0.031	0.00044	0.063	0.11	0.16	0.11	0.28
ρ	a_4	1.000	-0.395	0.485	0.895	-0.985	0.025	-0.605	-0.155	-0.575	-0.495
	a_5	-0.395	1.000	-0.935	-0.075	0.265	-0.075	-0.025	-0.185	-0.085	0.045
	a_{17}	0.485	-0.935	1.000	0.515	-0.575	-0.125	-0.345	0.145	-0.255	-0.405
	a_B	0.895	-0.075	0.515	1.000	-0.995	-0.115	-0.705	-0.005	-0.625	-0.505
	a_W	-0.985	0.265	-0.575	-0.995	1.000	-0.075	0.575	0.105	0.425	0.435
	a_G	0.025	-0.075	-0.125	-0.115	-0.075	1.000	0.235	-0.735	0.005	0.145
	Δa_C	-0.605	-0.025	-0.345	-0.705	0.575	0.235	1.000	0.345	0.785	0.535
	$\frac{Y_t^{(1)}}{Y_t^{(0)}} - 1$	-0.155	-0.185	0.145	-0.005	0.105	-0.735	0.345	1.000	0.465	0.165
	$\frac{Y_b^{(1)}}{Y_b^{(0)}} - 1$	-0.575	-0.085	-0.255	-0.625	0.425	0.005	0.785	0.465	1.000	0.535
	$\frac{Y_\tau^{(1)}}{Y_\tau^{(0)}} - 1$	-0.495	0.045	-0.405	-0.505	0.435	0.145	0.535	0.165	0.535	1.000
	$\frac{Y_\mu^{(1)}}{Y_\mu^{(0)}} - 1$	-0.225	0.005	-0.185	-0.215	0.145	-0.085	0.185	0.035	0.145	0.105

When compared to the corresponding analysis performed in the framework of SMEFT at dimension-six in the HISZ basis [57,58] the main difference is the contribution of the operator \mathcal{P}_{17} which has no linear sibling at dimension six. This operator leads to vertices $\partial^\mu H Z_\mu Z^\nu$ and $\partial^\mu H F_\mu Z^\nu$ and, generically its addition enlarges the

allowed range for the rest of the coefficients contributing to the Higgs-gauge-boson trilinear interactions. Therefore, it is mostly correlated with those coefficients which modify the HZZ and $H\gamma Z$ couplings as well, i.e., a_4 , a_5 , a_B , and a_W , as can be seen in the corresponding entries in Eq. (4.4) and it is graphically illustrated in Fig. 5.

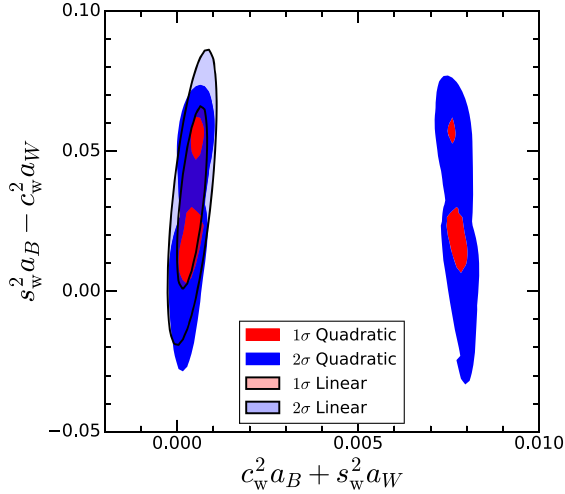


FIG. 4. 1 σ and 95% C.L. (2 d.o.f.) allowed regions from the Higgs analysis for the combinations $c_w^2 a_B + s_w^2 a_W$ and $s_w^2 a_B - c_w^2 a_W$. The results are shown for the analyses including only the linear contributions of the Wilson coefficients (lighter regions) as well as up to quadratic contributions (darker regions).

V. DISCUSSION

In this work we have presented the results of comprehensive analyses of low-energy electroweak precision measurements as well as LHC data on gauge boson pair production and Higgs observables in the context of the effective low-energy theory for a dynamical Higgs. We focused on observables related to the electroweak sector, which at present allow for precision tests of the couplings between electroweak gauge bosons and fermions, triple electroweak gauge couplings, and the couplings of the Higgs to fermions and gauge bosons. For the sake of assessing the impact of the Higgs kinematic distributions, we performed an analysis including the most updated STXS Higgs data in combination with the Higgs total signal strengths for those channels for which no kinematic information is available. In total, the analyses of EWPO and EWDBD and Higgs results from LHC run 2 encompass $15 + 73 + 101 = 189$ observables; see Sec. III for further details.

We worked in the framework of effective Lagrangians assuming the nonlinear (chiral) realization of the

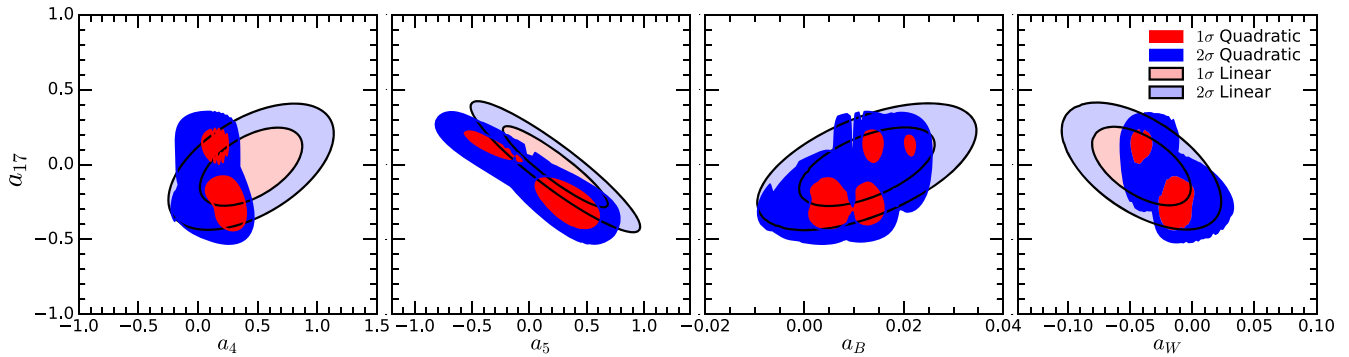


FIG. 5. 1σ and 95% C.L. (2 d.o.f) allowed regions from the Higgs analysis for $a_{17} \otimes (a_4, a_5, a_B, \text{ and } a_W)$, profiling over the undisplaced parameters. The results are shown for analyses including only the linear contributions of the Wilson coefficients (lighter regions) as well as up to quadratic contributions (darker regions).

electroweak gauge symmetry, the so-called HEFT which we have considered up to next-to-leading order. Under the flavor assumption that the new operators do not introduce additional tree-level sources of flavor violation nor violation of universality of the weak current, the analysis involves a total of 25 Wilson coefficients, of which ten are more severely constrained by EWPO, 4 in addition are constrained by EWDBD, and 11 are determined by the Higgs data analysis.

All of the analyses performed show no statistically significant source of tension with the SM. We find

$$\begin{aligned} \chi^2_{\min \text{ EWPO, SM}} &= 18.3, & 15 \text{ observables,} \\ \chi^2_{\min \text{ EWDBD SM}} &= 63.7, & 73 \text{ observables,} \\ \chi^2_{\min \text{ Higgs, SM}} &= 99.2, & 101 \text{ observables,} \end{aligned} \quad (5.1)$$

to be compared with

$$\begin{aligned} \chi^2_{\min \text{ EWPO, HEFT Linear}} &= 6, & 15 \text{ observables \& 10 coefficients,} \\ \chi^2_{\min \text{ EWDBD, HEFT Linear [HEFT Quadratic]}} &= 63[63], & 73 \text{ observables \& 4 coefficients,} \\ \chi^2_{\min \text{ Higgs, HEFT Linear [HEFT Quadratic]}} &= 89[87], & 101 \text{ observables \& 11 coefficients.} \end{aligned} \quad (5.2)$$

The results of the analysis can be confronted with those performed under different assumptions for the nature of the Higgs boson i.e., whether it is an isosinglet or a member of a $SU(2)_L$ doublet. In particular, as summarized in Sec. II, a particularly sensitive probe of the nature of the Higgs boson is associated with the (de)correlation of the contributions to TGCs and Higgs-gauge-boson couplings in the SMEFT and HEFT scenarios. This comparison can be quantified in terms of the four parameters in Eq. (2.27) [7,25]. Figure 6 shows the current status of the bounds on the two relevant planes of these coefficients.

The constraints of Σ_B , Σ_W , Δ_B , and Δ_W shown in Fig. 6 present a significant improvement with respect to the bounds previously shown in Fig. 3 of Ref. [25] in the Δ_B and Σ_B axis. They also show that the comparison between the two scenarios is robust irrespective of whether the analysis is performed at linear or quadratic order in the Wilson coefficients. We learn from this figure that, presently, the data gathered so far is not enough to distinguish between the two scenarios for the Higgs nature. From the right panel we read that the SMEFT lies within the 1σ allowed region of either the linear or quadratic analysis.

Up to now we have focused on a bottom-up approach where all the Wilson coefficients are treated as free parameters. Next, we consider the minimal composite Higgs models and perform an analysis in which only the deviations in Eqs. (2.28) and (2.30), parametrized by the unique GB scale parameter $\xi = v^2/f$, are allowed. We present in Fig. 7 the $\Delta\chi^2$ dependence on the GB scale, f , for several choices for the embedding of the SM top, bottom, tau, and muon into the UV-model. As we can see the least stringent bound of f originated for the choice (B, B, A, A) for (t, b, τ, μ) that reads $f > 1$ TeV at 95% C.L., while the strongest bound is for the choice (A, A, B, A) for (t, b, τ, μ) and implies $f > 1.45$ TeV. These results are in qualitative agreement with the bounds derived Ref. [24] with an slight improvement of about $\sim 10\%-20\%$ from the more up to date data samples considered. The results in the figure are shown for the analysis performed at linear order in the coefficients, but the analysis performed at quadratic order leads to very similar results. In particular this family of models do not allow for the realization of the degenerated solution with inverse sign of the couplings because, by

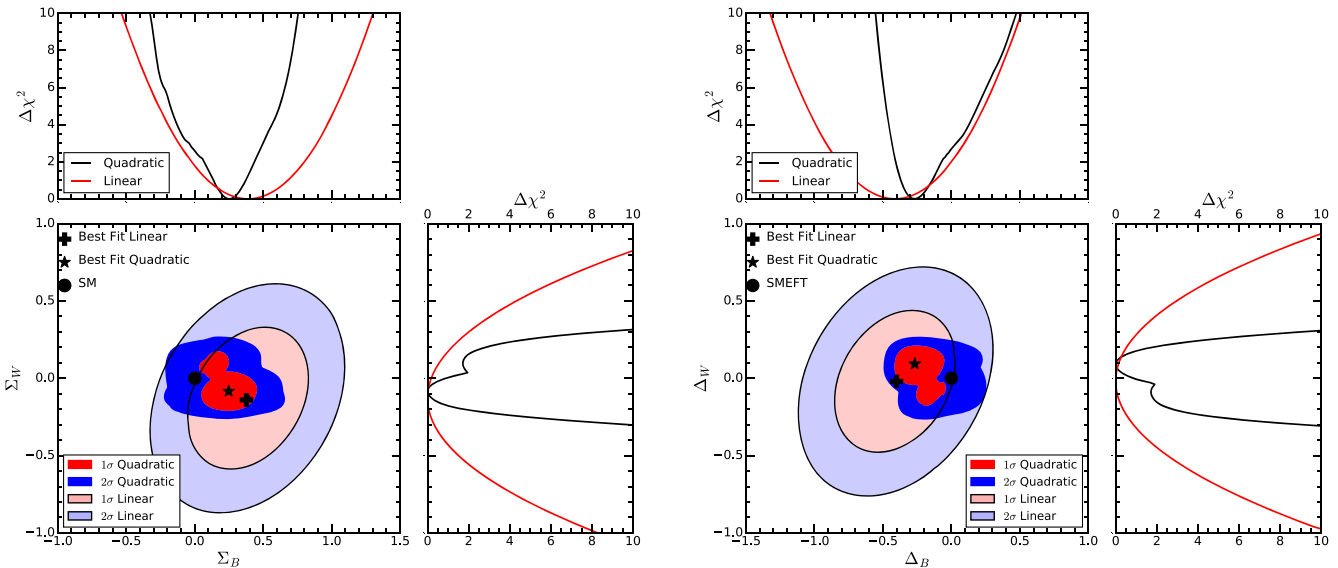


FIG. 6. Present bounds on Σ_B , Σ_W , Δ_B , and Δ_W (see text for the details on their definition) as obtained from the most recent combined global analysis of Higgs and EWDBD after profiling over the undisplayed parameters spanned in the analysis (Δa_C , a_B , a_G , a_W , a_{17} , $Y_t^{(1)}$, $Y_b^{(1)}$, $Y_\tau^{(1)}$, $Y_\mu^{(1)}$, c_{13} , and c_{WWW}).

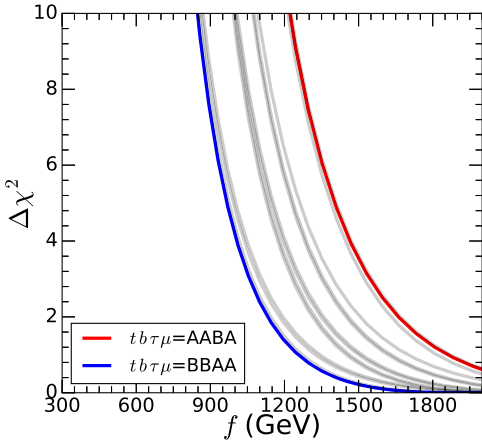


FIG. 7. $\Delta\chi^2$ as a function of the GB scale f for several choices of the SM fermions embedding in minimal composite Higgs models.

construction, the HVV and Hff couplings in these models have the same sign than in the SM. The constraints obtained for the minimal composite Higgs models also illustrate how specific UV-completions are subject to stronger bounds due to relations between the Wilson coefficients. For example, the marginalized 2σ allowed range in Table II for the top Yukawa implies an upper bound on $f > 460(800)$ for

models embedding A (B) which are about a factor ~ 2 weaker than the bounds in Fig. 7.

In summary, the increased integrated luminosity gathered at LHC run 2 allows for improved tests of electroweak symmetry breaking scenarios with a dynamical Higgs. We find no indication of statistically significant deviations from the SM predictions in the analysis of Higgs results and EWDBD. This, in combination with the EWPO, results into tighter constraints on the nature of the Higgs boson.

ACKNOWLEDGMENTS

M. M. thanks the hospitality of the Universitat de Barcelona where part of this work was done. This work is supported in part by Conselho Nacional de Desenvolvimento Científico e Tecnológico (CNPq) Grant No. 305762/2019-2, and by Fundação de Amparo à Pesquisa do Estado de São Paulo (FAPESP) Grants No. 2018/16921-1 and No. 2021/08669-3. M. C. G.-G. is supported by Spanish Grant No. PID2019-105614 GB-C21 financed by MCIN/AEI/10.13039/501100011033, by USA-NSF Grant No. PHY-1915093, and by AGAUR (Generalitat de Catalunya) Grant No. 2017-SGR-929. The authors acknowledge the support of European Innovative Training Networks Grant No. H2020-MSCA-ITN-2019//860881-HIDDeN.

[1] S. Weinberg, *Physica (Amsterdam)* **96A**, 327 (1979).

[2] H. Georgi, *Weak Interactions and Modern Particle Theory* (Benjamin/Cummings, Menlo Park, USA, 1984), ISBN 9780805331639.

[3] J. F. Donoghue, E. Golowich, and B. R. Holstein, *Dynamics of the Standard Model* (Cambridge University Press, Cambridge, England, 2014).

[4] G. Aad *et al.* (ATLAS Collaboration), *Phys. Lett. B* **716**, 1 (2012).

[5] S. Chatrchyan *et al.* (CMS Collaboration), *Phys. Lett. B* **716**, 30 (2012).

[6] I. Brivio and M. Trott, *Phys. Rep.* **793**, 1 (2019).

[7] I. Brivio, T. Corbett, O. J. P. Éboli, M. B. Gavela, J. Gonzalez-Fraile, M. C. Gonzalez-Garcia, L. Merlo, and S. Rigolin, *J. High Energy Phys.* **03** (2014) 024.

[8] D. B. Kaplan and H. Georgi, *Phys. Lett.* **136B**, 183 (1984).

[9] D. B. Kaplan, H. Georgi, and S. Dimopoulos, *Phys. Lett.* **136B**, 187 (1984).

[10] K. Agashe, R. Contino, and A. Pomarol, *Nucl. Phys.* **B719**, 165 (2005).

[11] G. Buchalla, O. Catá, and C. Krause, *Phys. Lett. B* **731**, 80 (2014).

[12] M. Gillioz, R. Grober, C. Grojean, M. Muhlleitner, and E. Salvioni, *J. High Energy Phys.* **10** (2012) 004.

[13] J. Ellis and T. You, *J. High Energy Phys.* **06** (2013) 103.

[14] A. Azatov, R. Contino, and J. Galloway, *J. High Energy Phys.* **04** (2012) 127; **04** (2013) 140(E).

[15] G. Buchalla, O. Cata, A. Celis, and C. Krause, *Eur. Phys. J. C* **76**, 233 (2016).

[16] T. Corbett, O. J. P. Éboli, D. Goncalves, J. González-Fraile, T. Plehn, and M. Rauch, *J. High Energy Phys.* **08** (2015) 156.

[17] H.-L. Li, L.-X. Xu, J.-H. Yu, and S.-H. Zhu, *J. High Energy Phys.* **09** (2019) 010.

[18] D. Liu, I. Low, and R. Vega-Morales, *Eur. Phys. J. C* **80**, 829 (2020).

[19] J. de Blas, O. Eberhardt, and C. Krause, *J. High Energy Phys.* **07** (2018) 048.

[20] D. de Florian *et al.* (LHC Higgs Cross Section Working Group), *arXiv:1610.07922*.

[21] J. R. Andersen *et al.*, in *Proceedings of the 9th Les Houches Workshop on Physics at TeV Colliders* (2016), *arXiv:1605.04692*.

[22] A. Banerjee, G. Bhattacharyya, N. Kumar, and T. S. Ray, *J. High Energy Phys.* **03** (2018) 062.

[23] V. Sanz and J. Setford, *Adv. High Energy Phys.* **2018**, 7168480 (2018).

[24] C. K. Khosa and V. Sanz, *arXiv:2102.13429*.

[25] I. Brivio, J. Gonzalez-Fraile, M. C. Gonzalez-Garcia, and L. Merlo, *Eur. Phys. J. C* **76**, 416 (2016).

[26] K. Hagiwara, R. D. Peccei, D. Zeppenfeld, and K. Hikasa, *Nucl. Phys.* **B282**, 253 (1987).

[27] M. Buschmann, C. Englert, D. Goncalves, T. Plehn, and M. Spannowsky, *Phys. Rev. D* **90**, 013010 (2014).

[28] M. Carena, L. Da Rold, and E. Pontón, *J. High Energy Phys.* **06** (2014) 159.

[29] S. Schael *et al.* (SLD Electroweak Group, DELPHI, ALEPH, SLD, SLD Heavy Flavour Group, OPAL, LEP Electroweak Working Group, L3 Collaborations), *Phys. Rep.* **427**, 257 (2006).

[30] C. Patrignani *et al.* (Particle Data Group), *Chin. Phys. C* **40**, 100001 (2016).

[31] L. E. W. Group (Tevatron Electroweak Working Group, CDF, DELPHI, SLD Electroweak and Heavy Flavour Groups, ALEPH, LEP Electroweak Working Group, SLD, OPAL, D0, L3 Collaborations), *arXiv:1012.2367*.

[32] M. Aaboud *et al.* (ATLAS Collaboration), *Eur. Phys. J. C* **78**, 24 (2018).

[33] CMS Collaboration, CERN Report No. CMS-PAS-SMP-20-014, 2021.

[34] A. M. Sirunyan *et al.* (CMS Collaboration), *Phys. Rev. D* **102**, 092001 (2020).

[35] CMS Collaboration, CERN Report No. CMS-PAS-SMP-20-005, 2021.

[36] ATLAS Collaboration, CERN Report No. ATLAS-CONF-2018-034, 2018.

[37] G. Aad *et al.* (ATLAS Collaboration), *Eur. Phys. J. C* **81**, 163 (2021).

[38] G. Aad *et al.* (ATLAS Collaboration), *J. High Energy Phys.* **06** (2021) 003.

[39] Atlas Collaboration, CERN Report No. ATLAS-CONF-2020-027, 2020.

[40] G. Aad *et al.* (ATLAS Collaboration), *Phys. Lett. B* **809**, 135754 (2020).

[41] G. Aad *et al.* (ATLAS Collaboration), *Phys. Lett. B* **812**, 135980 (2021).

[42] ATLAS Collaboration, CERN Report No. ATLAS-CONF-2020-053, 2020.

[43] CMS Collaboration, CERN Report No. CMS-PAS-HIG-19-005, 2020.

[44] CMS Collaboration, CERN Report No. CMS-PAS-HIG-19-014, 2021.

[45] A. M. Sirunyan *et al.* (CMS Collaboration), *J. High Energy Phys.* **07** (2021) 027.

[46] CMS Collaboration, CERN Report No. CMS-PAS-HIG-19-010, 2020.

[47] CMS Collaboration, CERN Report No. CMS-PAS-HIG-19-017, 2021.

[48] R. Frederix, S. Frixione, V. Hirschi, D. Pagani, H. S. Shao, and M. Zaro, *J. High Energy Phys.* **07** (2018) 185.

[49] N. D. Christensen and C. Duhr, *Comput. Phys. Commun.* **180**, 1614 (2009).

[50] A. Alloul, N. D. Christensen, C. Degrande, C. Duhr, and B. Fuks, *Comput. Phys. Commun.* **185**, 2250 (2014).

[51] T. Sjostrand, S. Mrenna, and P. Z. Skands, *Comput. Phys. Commun.* **178**, 852 (2008).

[52] J. de Favereau, C. Delaere, P. Demin, A. Giammanco, V. Lemaitre, A. Mertens, and M. Selvaggi (DELPHES 3 Collaboration), *J. High Energy Phys.* **02** (2014) 057.

[53] M. Cacciari, G. P. Salam, and G. Soyez, *Eur. Phys. J. C* **72**, 1896 (2012).

[54] V. Hirschi and O. Mattelaer, *J. High Energy Phys.* **10** (2015) 146.

[55] C. Degrande, G. Durieux, F. Maltoni, K. Mimasu, E. Vryonidou, and C. Zhang, *Phys. Rev. D* **103**, 096024 (2021).

[56] A. Buckley, J. Butterworth, D. Grellscheid, H. Hoeth, L. Lonnblad, J. Monk, H. Schulz, and F. Siegert, *Comput. Phys. Commun.* **184**, 2803 (2013).

[57] K. Hagiwara, S. Ishihara, R. Szalapski, and D. Zeppenfeld, *Phys. Rev. D* **48**, 2182 (1993).

- [58] K. Hagiwara, T. Hatsukano, S. Ishihara, and R. Szalapski, *Nucl. Phys.* **B496**, 66 (1997).
- [59] A. Pomarol and F. Riva, *J. High Energy Phys.* 01 (2014) 151.
- [60] T. Corbett, O. J. P. Éboli, and M. C. Gonzalez-Garcia, *Phys. Rev. D* **96**, 035006 (2017).
- [61] A. Alves, N. Rosa-Agostinho, O. J. P. Éboli, and M. C. Gonzalez-Garcia, *Phys. Rev. D* **98**, 013006 (2018).
- [62] E. d. S. Almeida, A. Alves, O. J. P. Éboli, and M. C. Gonzalez-Garcia, *Phys. Rev. D* **105**, 013006 (2022).
- [63] A. Azatov, J. Elias-Miro, Y. Reymuaji, and E. Venturini, *J. High Energy Phys.* 10 (2017) 027.
- [64] A. Azatov, D. Barducci, and E. Venturini, *J. High Energy Phys.* 04 (2019) 075.